applied sciences

MDPI

Article

Bearing Fault Diagnostics Based on the Square of the Amplitude Gains Method

Rafał Grądzki [1,*], Błażej Bartoszewicz [1] and José Emiliano Martínez [2]

[1] Faculty of Mechanical Engineering, Bialystok University of Technology, Wiejska st. 45C, 15-351 Bialystok, Poland
[2] Department of Engineering Studies for Innovation, Universidad Iberoamericana Ciudad de México, Prol. Paseo de la Reforma 880, CDMX 01219, Mexico
* Correspondence: r.gradzki@pb.edu.pl

Abstract: The article presents an adaptation of a parametric diagnostic method based on the square of the amplitude gains model, which was tested in experimental studies on bearing damage detection (outer race, inner race, bearing balls damage). The described method is based on the shaft displacement signal analysis, which is affected by vibrations coming from the bearings. The diagnostic model's parameters are determined by processing the signal from the time domain to the frequency domain in a few steps. Firstly, the recorded signal is divided into two observation periods, next the analytical autocorrelation functions are determined and approximated by a polynomial. Then, the diagnostic thresholds are adopted, and the model parameters are converted into damage maps that are easy to interpret and assess the technical condition of the bearings. The presented method shows the technical condition of bearings in a qualitative way. Depending on the received color damage maps, it is possible to determine their level of wear. *Green* and *blue* indicate poor wear or no damage, *red* indicates increased wear, and *black* clearly indicates a damaged bearing.

Keywords: bearing; bearing outer race; bearing inner race; diagnostic model; diagnostics; bearing damage; the square of the amplitude gain

Citation: Grądzki, R.; Bartoszewicz, B.; Martínez, J.E. Bearing Fault Diagnostics Based on the Square of the Amplitude Gains Method. *Appl. Sci.* **2023**, *13*, 2160. https://doi.org/10.3390/app13042160

Academic Editors: Jose Machado and Emanuele Carpanzano

Received: 19 December 2022
Revised: 19 January 2023
Accepted: 1 February 2023
Published: 8 February 2023

1. Introduction

Bearing failure diagnostics is an important part of rotating machinery maintenance. Accurate and early bearing damage detection contributes to safer and more efficient machine exploitation [1–12].

Following many hours of bearing operation, the impact of excessive vibrations in combination with limited lubrication of machine parts leads to bearing damage: outer race, inner race, damage to the cage, and rolling elements (balls). If left undetected for some time, this mechanical damage can cause equipment failure and, consequently, unscheduled downtime. Therefore, timely intervention or preventive maintenance is vital to keeping rotating equipment running efficiently.

Recently, there have been many techniques that can be used to monitor bearing health, such as vibration monitoring [13–29], noise monitoring [30–32], temperature monitoring [33–35], and residual wear analysis [36–39]. However, vibration monitoring is the most effective technique—single-point defects produce successive pulses with each contact of the damage with the rolling element, and each contact can excite a high-frequency resonance in the overall structure. The mentioned analysis allows for detecting, locating, and distinguishing various types of damage from the moment of its occurrence before they become critical and dangerous. These damages can be dispersed or localized [22].

Unfortunately, the vibration signal does not only contain signals originating directly from the bearing. It also contains vibration signals from cooperating elements, e.g., shafts or another mechanism. Their misalignment, unbalance, stiffness, clearance, and friction will also affect the recorded signal coming from the bearings. Therefore, modern diagnostics

require techniques of advanced signal processing: fast Fourier transform (FFT) [40–50], cepstrum analysis (CA) [51–53], short time Fourier transform (STFT) [54,55], Wigner–Ville Distribution (WVD) [54–56], the envelope analysis (EA) [57,58], and wavelet transform (WT) [58–62], and various advanced models based on artificial intelligence [63–80].

Vibration data analysis mainly includes the time domain, frequency domain, time-frequency domain, and other analysis methods, but the vast majority are based on time-frequency analysis.

The authors also developed time-frequency methods. In their work, they proved the effectiveness of parametric methods: in the form of a square signal amplitude amplification and an original model in the form of a difference in phase shifts of signals for diagnosing shafts and compressors of aircraft engine turbines.

A mathematical model of a square of amplitude gains for diagnostic purposes was first presented in 2004 [81]. Lindstedt and Kotowski presented its application for detecting damage to an aircraft engine blade in stationary conditions (removal of the blade from the engine required). The vibration signal was generated by modal hammer impact. In 2007, Kotowski and Lindstedt [82] presented a complete study with an analysis of the impact of this model's parameters on the damage type and location.

The next stage of the method development took place at the Air Force Institute of Technology (ITWL) in Warsaw (Poland) in 2009 [83,84]. The article presents the mathematical basis for adapting the method to diagnostics during a rotating machine operation. However, this approach has not been experimentally verified. In 2010, Lindstedt and Grądzki [85] determined the parameters of the diagnostic model from the recorded signal from the inductive sensor. In 2012, Grądzki [86] in his doctoral thesis, presented extensive research on the compressor blade of the S0–3 turbine engine during its operation. An analysis of the impact of changes in the environment represented by the rotational speed on the changes of model parameters was carried out, and color damage maps were used to analyze the technical condition. For verification, a new diagnostic model in the form of a difference in phase shifts of signals was also developed and tested. Endoscopic measurements additionally verified all results.

In 2018, the authors [87], using a parametric diagnostic model of a difference in phase shifts of signals, presented an analysis of the technical condition of the entire rim of SO-3 compressor blades. In 2020 [88], they presented another model modification, which allowed both to examine the technical condition of the blade and its stationary condition during operation.

The model of a square of amplitude gains has also been implemented for shaft diagnostics during their operation [89]. The authors showed the effectiveness of the damage map to verify the different types of shaft damage in simulation and experimental research.

In the presented article, the authors adapted the square of amplitude gains method to detect bearing damage (outer race, inner race, bearing ball damage at different depths). Firstly, a recorded signal of shaft displacement is divided into two observation periods. Then, the analytical autocorrelation functions are determined and approximated by a polynomial. On their basis, the Fourier transform is used to convert to the spectral (frequency) form. Thanks to this, it is possible to determine the parameters of the model to which fixed statistical diagnostic thresholds are assigned. The last step is to convert the model parameters into color damage maps that are easy to analyze and interpret.

At this stage, the proposed method allows for early detection of bearing technical conditions (damaged or undamaged). However, based on the parameter values, the authors cannot indicate the type of damage.

The article is presented as follows: The introduction is presented in Section 1. Section 2 describes the mathematical procedure for determining the model's parameters and obtaining color damage maps of the bearings. Section 3 presents the measurement stand and describes the objective and scope of the tests. Section 4 presents the experimental results of the tests carried out and compares the results obtained (by using FFT analysis and a square

of the amplitude gains method) for the undamaged and damaged bearings. Conclusions and discussions are in Section 5.

2. Condition Monitoring Based on the Squared Amplitude Gain of Signals

The mathematical foundations of the method are described in detail in [89].

To use the proposed diagnostic model to monitor the condition of the bearings, signals of rotor displacements near the supporting bearings during machine operation are measured and sampled. It is assumed that the rotor is undamaged, its state remains unchanged, and various bearing damage variants are introduced simultaneously. In this way, researchers determine the condition of the bearings, using the method described in the article based on the rotor displacement signals. Finally, as a result of using the method, damage maps characterizing the technical condition of the bearings are obtained.

In the first step of analyzing the signals obtained from the experimental studies, the time interval T_{02}, hereinafter referred to as a cycle, is determined for every single revolution. This interval corresponds to a full revolution of the shaft reduced on the outer parts of the intervals by several samples so that successive cycles do not overlap. Then the interval T_{02} is divided into two separate time intervals T_{01} and T_{12} (sample sets). Point T_1 is common for both ranges and marks the moment when the shaft surface is farthest from the sensor face (Figure 1).

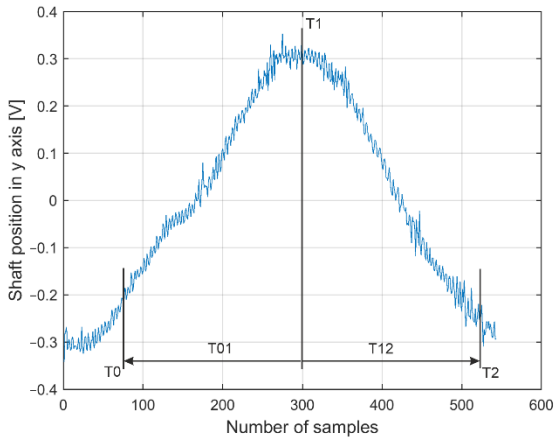

Figure 1. Dividing the signal into two sub-periods T_{01} and T_{12}.

Each cycle's number of signal samples must be identical and selected to ensure the proper statistical evaluation of the measured operational signals. For the tested rotational speed, the intervals T_{01} and T_{12} contain the same number of signal samples, and these intervals do not overlap. Frequency leakage was reduced by scaling each interval by a Hanning window.

For the displacement signal $y(t)$ in the assumed time intervals T_{01} and T_{12}, estimates of the autocorrelation functions ${R_{yy}}^{T01}$ and ${R_{yy}}^{T12}$, are determined, which are then approximated by analytical expressions (polynomials), ensuring a fit above 0.997.

The correlation function takes the form:

$$R_{yy}(\tau) = a_n\tau^n + \ldots + a_4\tau^4 + a_3\tau^3 + a_2\tau^2 + a_1\tau + a_0 \quad (1)$$

where: $a_0, a_1, \ldots\ a_n$—coefficients of the polynomials, $n = 0, 1, 2, 3, \ldots, r$.

The order n of the polynomials should be selected carefully—a too low order will result in inaccurate approximations, a too high order will result in an excessive number of polynomial coefficients and longer calculation times.

The described parametric diagnostic model is based on the functions of the spectral density of the power of the registered rotor vibration signal $y(t)$ in two time intervals (T_{01}, T_{12}) and the environment $x(t)$. It is assumed that the rotor work signals $y(t)$ and the envi-

ronment $x(t)$ are stochastic and the disturbed time courses are expressed by autocorrelation functions $R_{xx}(\tau)$ and $R_{yy}(\tau)$.

Based on the analytical forms of the auto-correlation function, the corresponding power auto-spectral density functions ${S_{yy}}^{T01}(j\omega)$ and ${S_{yy}}^{T12}(j\omega)$ are determined using the Fourier transform:

$$S_{yy}^{T01}(j\omega) = F(R_{yy}^{T01}(\tau)) \tag{2}$$

$$S_{yy}^{T12}(j\omega) = F(R_{yy}^{T12}(\tau)) \tag{3}$$

In the next step, it is assumed that the power densities of the environment signal $x(t)$ in time T_{01}, T_{12}–${S_{xx}}^{T01}(j\omega)$, and ${S_{xx}}^{T12}(j\omega)$ have been determined (in the same way as S_{yy}). Since the observation times are very close to each other, it can be assumed that the environment has not changed at that time; therefore ${S_{xx}}^{T01}(j\omega) \cong {S_{xx}}^{T12}(j\omega)$. Based on the above condition, a parametric diagnostic model can be determined in the form of the quotient of the power density function (square of the amplitude gains), allowing to eliminate the environment:

$$A^2_{T12T01}(\omega) = \frac{\frac{S_{yy}^{T12}}{\cancel{S_{xx}^{T12}}}}{\frac{S_{yy}^{T01}}{\cancel{S_{xx}^{T01}}}} \xrightarrow{S_{xx}^{T12} \cong S_{xx}^{T01}} \frac{S_{yy}^{T12}}{S_{yy}^{T01}} = \frac{A_0^* + A_1^* s + A_2^* s^2 + \ldots + A_n^* s^n}{B_0^* + B_1^* s + B_2^* s^2 + \ldots + B_n^* s^n} \tag{4}$$

where: s—complex variable, $s = j\omega$; ${A_i}^*$, $i = 0, 1, \ldots, n$—numerator estimates parameters; ${B_i}^*$, $i = 0, 1, \ldots, n$—denominator estimates parameters; n—polynomial order.

Despite the elimination of the environment, the parameters of the ${A^2}_{T12T01}$ model are directly related to the change in the technical condition of the rotor system supported on bearings. Therefore, a characteristic feature of the ${A^2}_{T12T01}$ model is that it does not require the measurement of environmental signals. However, it is indirectly considered by conducting diagnostic tests (two observation periods, determining the diagnostic model as a quotient of diagnostic models combining diagnostic signals and any environment with technical condition parameters).

Parameters of the numerator (A_i) and denominator (B_i) of the model are determined for each cycle of the rotating shaft, thus creating a matrix of parameters, describing the technical condition of the bearings during the operation-a damage map. The mean value μ and the standard deviation σ are determined for the corresponding model parameters from each cycle (e.g., A_0 for each cycle—the first column in the matrix of parameters). On their basis, statistical diagnostic thresholds of the forms $\mu \pm \sigma$, $\mu \pm 2\sigma$, $\mu \pm 3\sigma$ are determined.

Then, the determined values of Ai and Bi parameters are compared to the determined diagnostic thresholds and changed to the appropriate color (Table 1), creating the so-called damage maps of the technical condition of the object:

- *green* color if the parameter value did not exceed $\mu \pm \sigma$,
- *blue* color if the parameter value exceeded $\mu \pm \sigma$,
- *red* color if the parameter value exceeded $\mu \pm 2\sigma$,
- *black* color if the parameter value exceeded $\mu \pm 3\sigma$.

Table 1. Legend for the damage maps.

The Predominant Color in the Damage Map	Technical Condition	Stationary Condition
Black and *red*	"Serious failure"	"Strong" changes of bearing technical condition
Red	"Excessive wear"	"Weak" changes of bearing technical condition
Green and *blue*	"Slight or no wear"	"Slight" changes of bearing technical condition

This way, a damage map of the bearing is obtained, showing its technical condition. For example, if there are many *black* colors, the bearing is damaged, *red* means increased bearing wear, and *green* and *blue* colors mean little or no wear. This approach shows an unambiguous picture of the bearing damage assessment.

3. Experimental Test Stand

The proposed damage detection method was experimentally verified on the stand operated at the Bialystok University of Technology (Figure 2 and Table 2). The main element of the test stand is the rotor mounted on two ball bearings (1a–on the brake side and 1b–on the drive side), driven by an electric motor (2) with adjustable speed (up to 2000 rpm). The rotor consists of three parts: the middle part is a replaceable shaft (3), and the outer parts are the drive shaft and the braking shaft supported on the bearings. The shafts are connected into one rotor using conical fits and flanges with bolts ensuring, on the one hand, the axial symmetry of the rotor and, on the other, quick and simple reconfiguration of the shafts. Mass discs (4) are attached to the outer shafts. At the shaft's end, an electromagnetic brake (7) enables the torsional load introduction. The radial positions of the shaft near both bearings are measured by eddy current sensors placed in the horizontal and vertical planes, two at each bearing. Variants of the bearing damage were implemented in the support closer to the drive (1b).

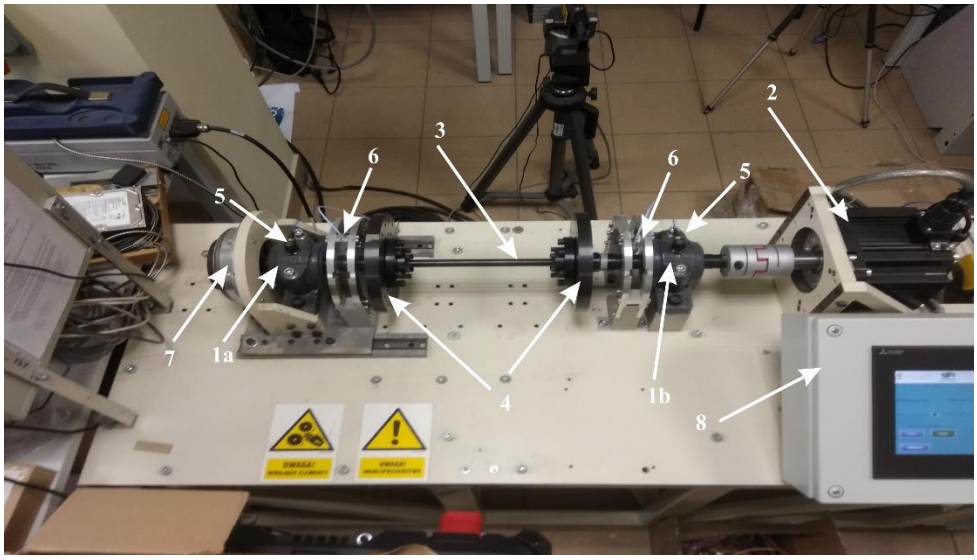

Figure 2. Measurement test rig: 1—ball bearings (a—on the brake side, b—on the drive side); 2—motor; 3—shaft; 4—mass disc; 5—accelerometers; 6—eddy current sensors; 7—electromagnetic brake; 8—control panel.

Table 2. Experimental test stand parameters.

Parameter Description	Value [Unit]
Bearing type	SKF 1207K EKTN9
Rotational speed	max 2 000 [rpm]
Shaft critical speed	3200 [rpm]
Load torque	No external forces
Radial force	
Sampling time	60 [s]
Sampling rate	8192 [Hz]

The object of the tests was the SKF 1207K bearing (Figure 3) with the parameters listed in Table 3:

Table 3. Parameters of ball bearing SKF 1207K EKTN9 [90].

Parameter	Value [Unit]
Manufacturer's model	1207 EKTN9
Outer diameter	72 [mm]
Inner diameter	35 [mm]
Outer ring periphery diameter	60.9 [mm]
Inner ring periphery diameter	47 [mm]
Width	17 [mm]
Weight	0.32 [kg]

The bearings were tested in five configurations: undamaged, with cut outer and inner race, with the cut ball at a depth of 1, 2, and 3 mm and width 0.3 mm. The registration of the diagnostic signals was implemented by eddy current sensors, positioned radially to the rotating shaft in the vertical Y and horizontal X axes (two sensors at each bearing).

The tested bearing is shown in Figure 3a and the types of its damage are presented in Figure 3b–f.

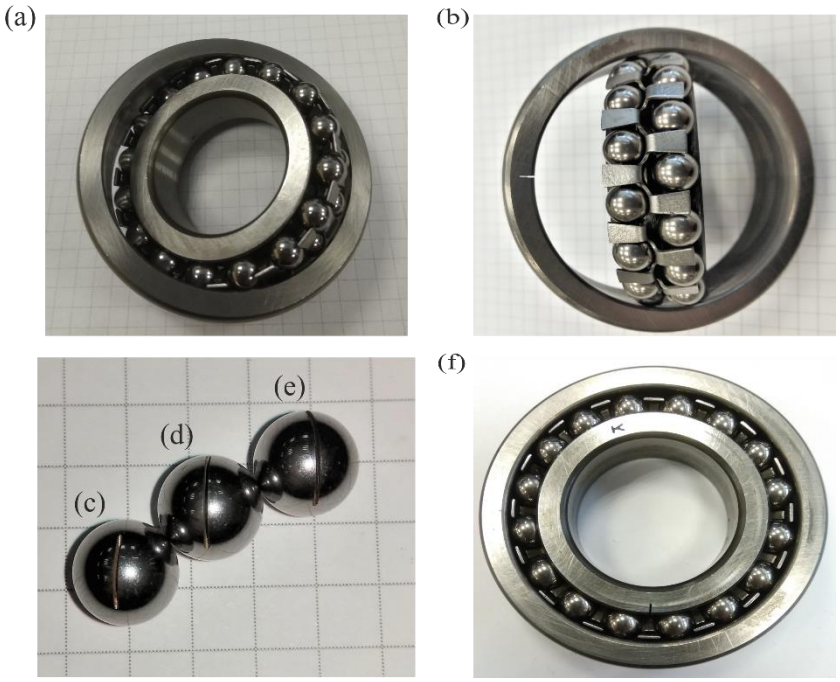

Figure 3. Ball bearing SKF 1207K: (**a**) undamaged; (**b**) with cut outer race; with the cut ball at the depthof: (**c**) 1 mm; (**d**) 2 mm; (**e**) 3 mm; (**f**) with cut inner race.

4. Experimental Results

To better show the type and influence of the simulated bearing faults on the measured vibrations, the authors prepared an FFT analysis of all damage signals for 900 rpm.

The frequencies of bearing 1207K, calculated for speed 900 rpm, are shown in Table 4:

Table 4. Frequencies of ball bearing SKF 1207K EKTN9 [90].

Parameter	Value [Unit]
Rotational frequencies:	
Inner ring	15 [Hz]
Outer ring	0 [Hz]
Rolling element set and cage	6.285 [Hz]
The rolling element about its axis	44.581 [Hz]
Frequencies of over-rolling:	
A point on the inner ring	130.72 [Hz]
A point on the outer ring	94.28 [Hz]
Rolling element	89.162 [Hz]

Based on the expected frequencies (Table 4) and the obtained frequency characteristics (Figures 4 and 5), the bearing faults are visible. However, the damages are not significant in the frequency characteristics, this is due to the narrow cut on the bearing elements. More significant bearing faults are visible in the amplitude change and new frequencies appearance [41]. However, the authors wanted to introduce minor damage.

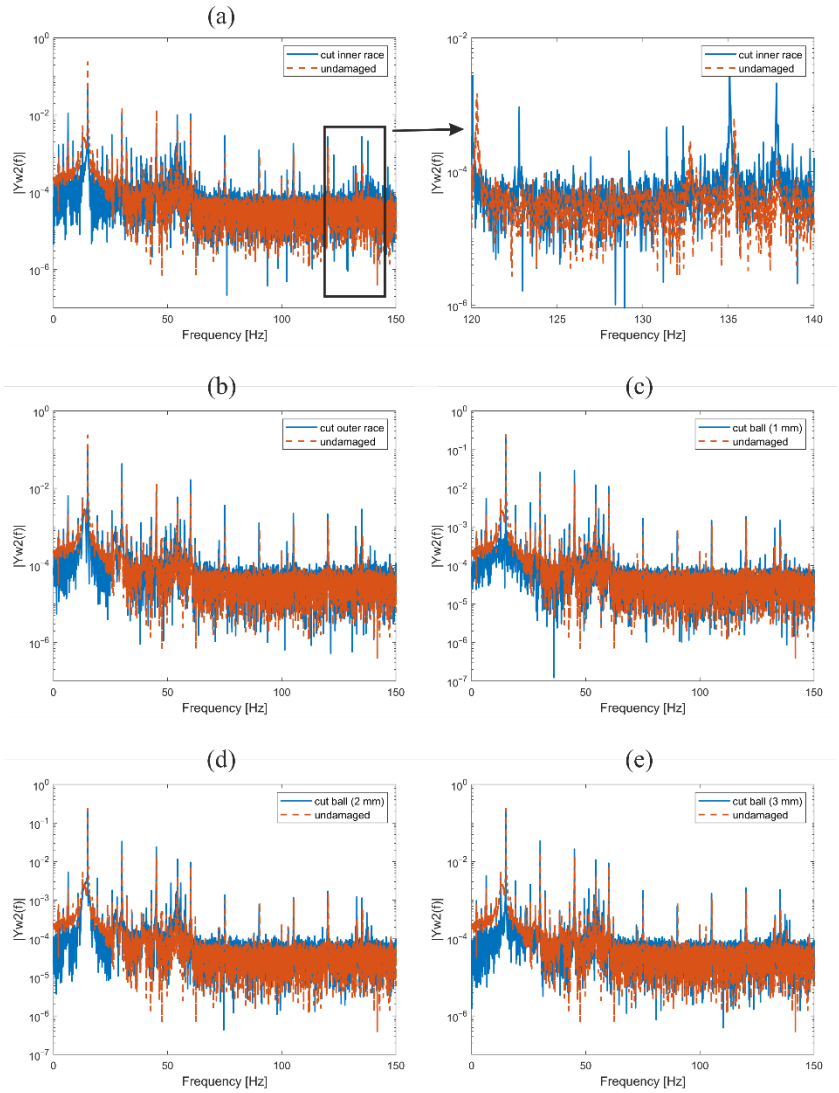

Figure 4. The FFT analysis of the recorded shaft displacement signal influenced by the vibration signal coming from bearing (drive side) SKF 1207K: (**a**) with cut inner race; (**b**) with cut outer race; with the cut ball at the depth of: (**c**) 1 mm; (**d**) 2 mm; (**e**) 3 mm.

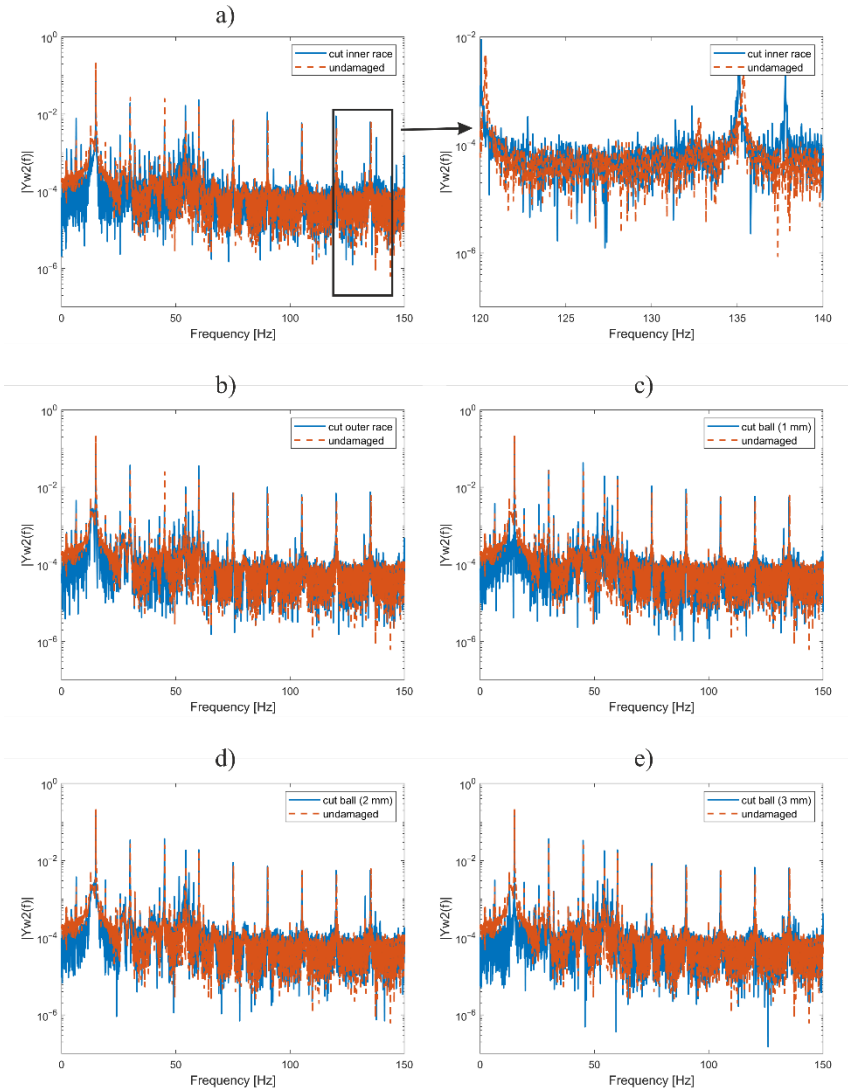

Figure 5. The FFT analysis of the recorded shaft displacement signal influenced by the vibration signal coming from bearing (brake side) SKF 1207K: (**a**) with cut inner race; (**b**) with cut outer race; with the cut ball at the depth of: (**c**) 1 mm; (**d**) 2 mm; (**e**) 3 mm.

Upon determining the frequency characteristic, the analysis was carried out using a squared amplitude gain method.

Examples of displacement signals of one shaft revolution obtained at the sampling frequency of 8192 Hz for each variant of bearing damage are shown in Figure 6.

The recorded experimental signals included the course of shaft vibrations during rotation for 60 s after the stabilization of the set rotational speed. In addition, measurements were carried out for rotational speeds from 100 every 100 to 2000 rpm and for each damage variant.

The shaft vibration signal from each sensor, containing many successive shaft revolutions, was divided into single revolutions. The analysis of the results was presented for the rotational speed of 900 rpm, and the signals were recorded for eddy current sensors located radially to the shaft in the vertical axis.

For the exemplary speed of 900 rpm, 900 cycles were obtained, corresponding to the number of shaft revolutions per minute. In each analysis, the first and last cycles were discarded, assuming they could represent an incomplete shaft rotation. For each of the cycles, the procedure was performed following the description of the model (Section 2). First, the Hanning window was used, and then the signal autocorrelation was determined.

The autocorrelation result was approximated by a polynomial, where the coefficient of determination R2 measured the level of the polynomial fit. Following some preliminary calculations, the order of approximating polynomials of the auto-correlation function was chosen as $n = 5$, which gives the coefficient of determination $R^2 > 99.97\%$. Adoption of the lower orders of polynomials leads to lower values of the coefficients of determination (i.e., less accurate approximations). Higher orders do not noticeably improve the approximation accuracy (because it is already close to 1), but they significantly extend the calculation time and the number of coefficients to analyze.

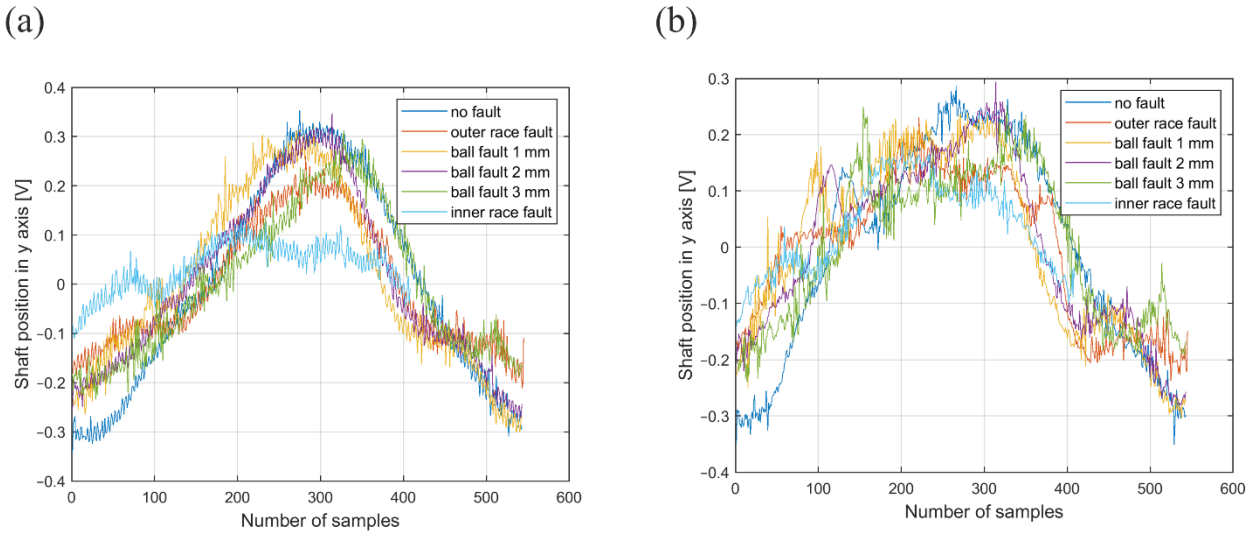

Figure 6. The recorded shaft displacement signal influenced by the vibration signal coming from the bearing: (**a**) from the brake side; (**b**) from the drive side.

Examples of auto-correlation functions and their fifth-order polynomial approximations in two observation zones of the selected cycle of the rotor displacement signal (from Figure 1) are shown in Figure 7.

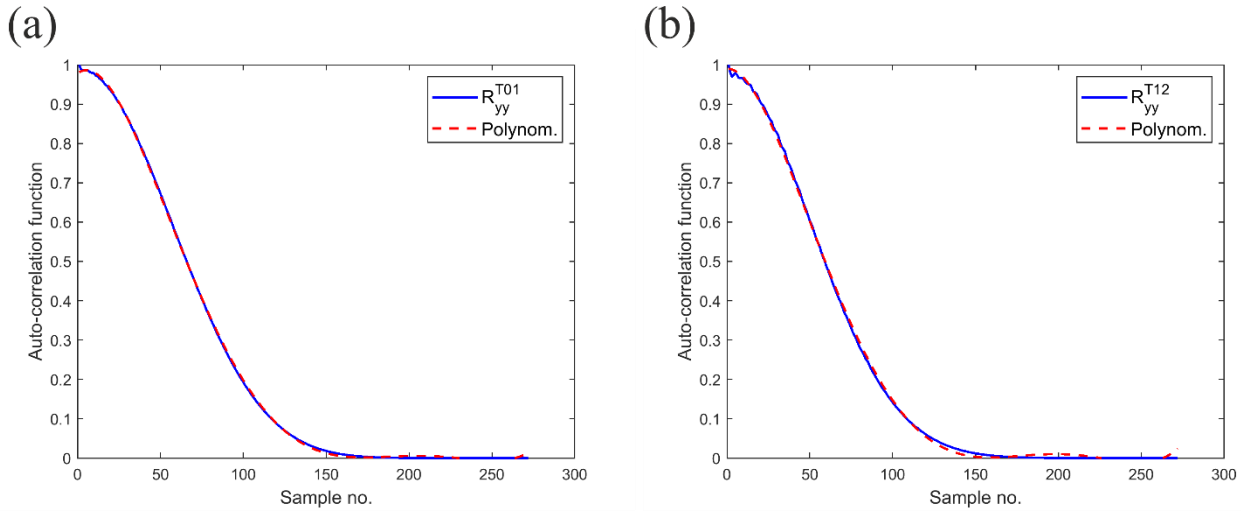

Figure 7. Auto-correlation signal for the rotor supported on the SKF 1207K bearing (with the ball cut on a depth of 1 mm) with the matching curve: (**a**) during the observation period T_{01}; (**b**) during the observation period T_{12}.

The damage map of the bearing technical condition consists of the 30 cycles, randomly selected (which is a statistical sample) from all (for a speed of 900 rpm, 900 cycles) recorded cycles, for a given speed. It is expected that the damage maps obtained for each draw will

give the same picture of the technical condition of the bearing (which will confirm the method's effectiveness).

First, a damage map was created for the undamaged bearing. The diagnostic thresholds set for it were the reference thresholds used for damaged bearings. The damage map contains 30 rows marked with numbers of randomly selected cycles and 12 columns, which consist of coefficients of 5th-order polynomials (six coefficients each) for the numerator and denominator of the model. Comparing the model results for different damage variants is possible, using only the same degree of the matching polynomial. The numbers of the damaged bearings cycles were the same as for the previously randomly selected cycles of the undamaged bearing.

The technical condition of the bearing is represented by 12 coefficients: six in the first observation period (T_{01}) and six in the second observation period (T_{12}). These zones are visible as the left and right parts of the technical condition damage maps (Figures 8a–f and 9a–f), separated by a thick black line.

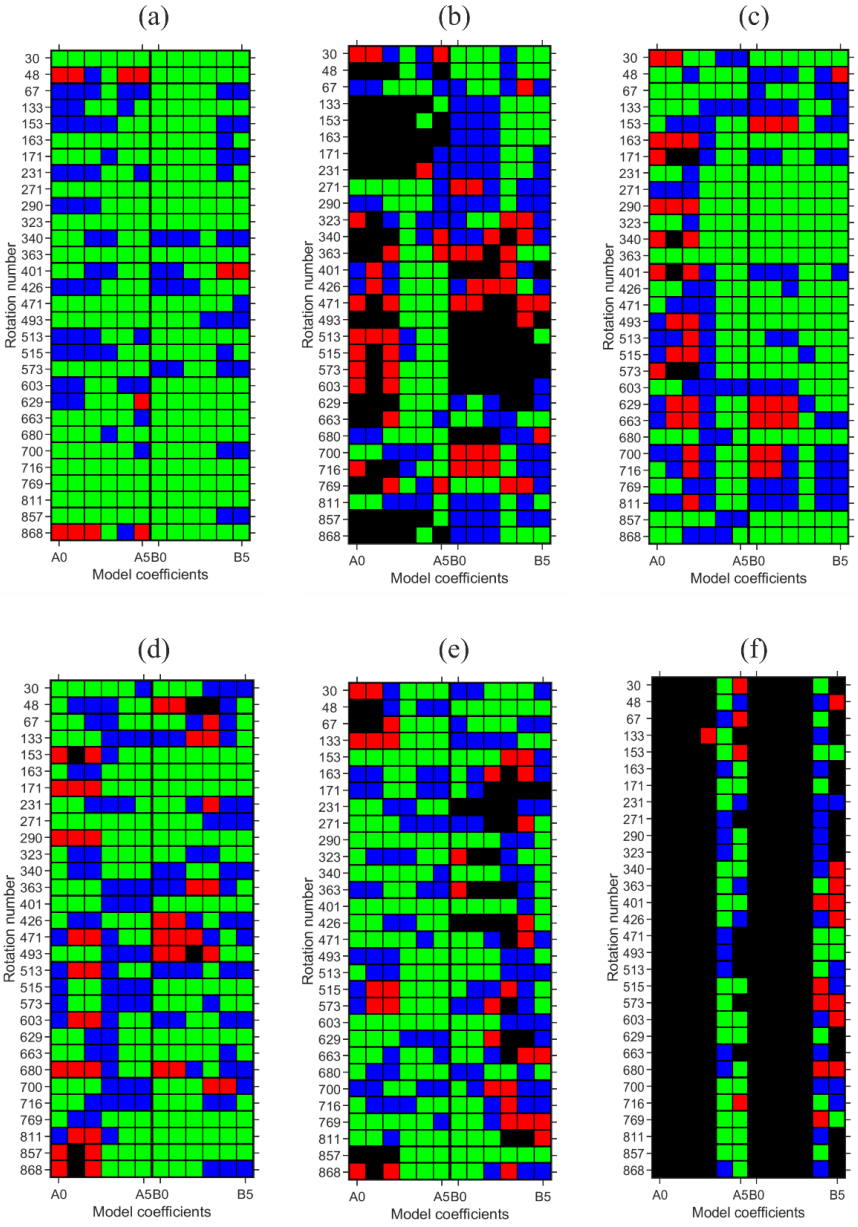

Figure 8. The damage map of bearing (drive side) SKF 1207K: (**a**) undamaged; (**b**) with a damaged outer race; with the cut ball at the depth of: (**c**) 1 mm; (**d**) 2 mm; (**e**) 3 mm; (**f**) with cut inner race.

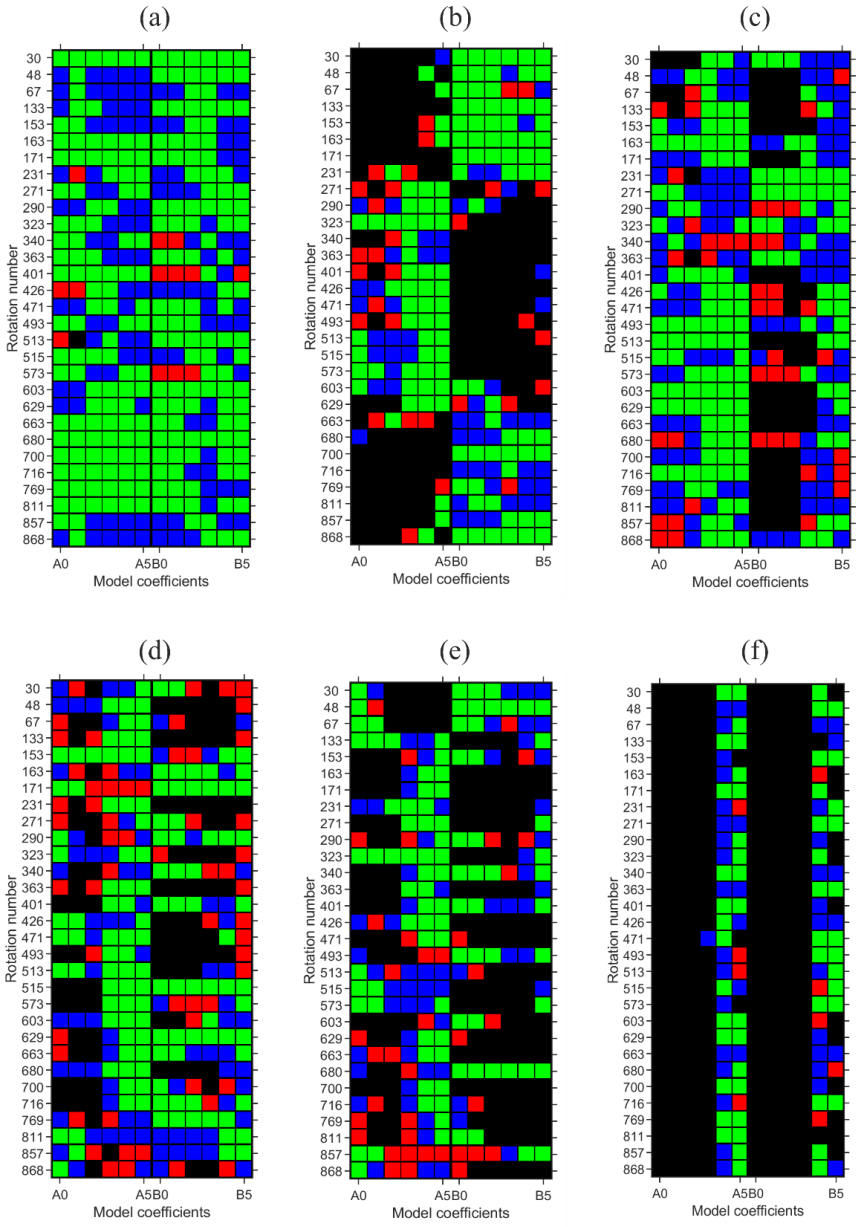

Figure 9. The damage map of bearing (brake side) SKF 1207K: (**a**) undamaged; (**b**) with a damaged outer race; with the cut ball at the depth of: (**c**) 1 mm; (**d**) 2 mm; (**e**) 3 mm; (**f**) with cut inner race.

Based on Figures 8 and 9, it can be seen that the technical condition of each bearing is clearly and unambiguously indicated on the damage maps obtained. Dominant *red* and *black* fields are characteristic of severely damaged bearings. Moreover, the undamaged bearing is dominated by *blue* and *green*. Since damage thresholds are based on statistics, slight variations between the colors of a given damage map are possible. Therefore, it is important to analyze the map globally for a reasonable number of rotation cycles (map rows).

Damage maps can present the technical condition of all analyzed bearings in a concise, graphical form. Based on the generated maps (Figures 8 and 9), it is possible to present a quantitative form of the technical condition. Collective graphs of quantitative analysis (Figure 10) will facilitate the comparison of damage maps in terms of the increase in the number of *black* and *red* fields and the decrease in *green* in relation to the increasing damage.

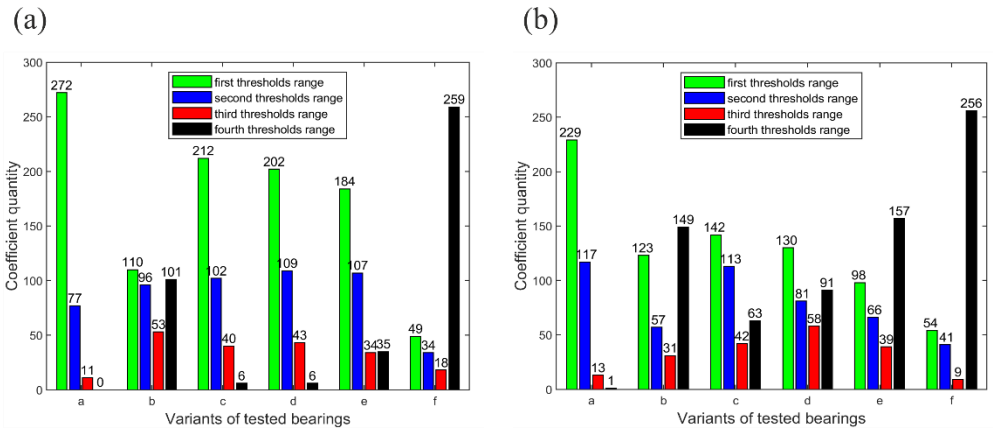

Figure 10. Collective characteristics of the damage maps of the SKF 1207K bearing from the side of: (**a**) the drive (**b**) the brake for the shaft speed of 900 rpm.

Figure 10 presents a quantitative summary of all tested bearing variants at the rotor speed of 900 rpm (Figure 10a-bearing closer to the brake, 10b-bearing closer to the drive). Bearing variants are marked on the horizontal axis (a–undamaged bearing; b–with a damaged outer race; with the cut ball at the depth of: c–1 mm; d–2 mm; e–3 mm; f–with a damaged inner race), and on the vertical axis the number occurrences of a given color. It can be seen in both types of figures that the undamaged variant significantly dominates over the others in the case of the threshold not exceeding $\mu \pm \sigma$ (*green*), while the values of the thresholds indicating damage have the lowest. It can also be noticed that in the case of bearing balls with cuts 1, 2 and 3 mm deep, the threshold $\mu \pm \sigma$ decreases (*green*) while the threshold $\mu \pm 2\sigma$ increases (*black*). High values of *black* and *red* colors are visible for the variant of the bearing's outer race damage, as a result of which, during the rotation of the shaft, all of the balls in the bearing hit the discontinuity of the race, generating vibrations. The highest values of *black* color can be seen for the bearing with the cut inner race. In this case, balls more frequently hit the cut point on the inner race than in the outer race.

Summarizing the results presented in the collective characteristics (Figure 10), the number of occurrences of the *black*, *red*, *blue*, and *green* color fields is collected in Table 5. As can be seen from the damage maps, where the damage to the ball was 1 mm deep (Figure 9c) and 2 mm deep (Figure 9d), it is difficult to see an increase in the number of parameters. Therefore, a good complement to the damage maps of the technical condition is their quantitative analysis, from which it is already clear that there was an increase in the number of *red* and *black* fields between the indicated damage.

Table 5. Number of color fields in subsequent damage maps presented in Figures 8 and 9.

Selection	Bearing No 1				Bearing No 2			
	black	*red*	*blue*	*green*	*black*	*red*	*blue*	*green*
Undamaged bearing	0	11	77	272	1	13	117	229
Damaged outer race	101	53	96	110	149	31	57	123
Cut ball at a depth of 1 mm	6	40	102	212	63	42	113	142
Cut ball at a depth of 2 mm	6	43	109	202	91	56	81	130
Cut ball at a depth of 3 mm	35	34	107	184	157	39	66	96
Damaged inner race	259	18	34	49	256	9	41	54

The presented results reflect the technical condition of the bearing. In its current form, the method cannot determine the type of bearing damage based on the damage map, e.g., damage to the bearing ball to a depth of 1 or 3 mm. However, it is very effective for detecting when a bearing goes from a usefulness condition to failure (damage).

5. Summary

The parametric method of bearing failure detection presented in the article is based on auto-correlation and power spectral density functions. The signal is analyzed in two separate periods. When the space between the analyzed intervals is close to each other, the influence of external disturbances is eliminated. Therefore, each change in the parameters of the diagnostic model should be interpreted as a change in the machine's technical condition.

Markings of bearing damage are decipherable and presented in the form of characteristic color maps, where dominant *green* and *blue* indicate an undamaged bearing or very low wear, *red*—increased wear, or *black*—bearing damage. The exact location of the colors on the damage maps may vary as the diagnostic thresholds are determined by the mean and standard deviation, i.e., statistical parameters. Therefore, it is not the exact locations that are important but the predominance of a particular color. It should also be noted that the described parametric method should not be used on small datasets because it requires the determination of diagnostic thresholds based on statistical operations.

The experimental results confirmed that the method can reliably detect bearing damage. Furthermore, the method is simple and uses only measured vibration data (signal from one sensor is sufficient). Therefore, preliminary preparation of the rotor for testing is not required. Furthermore, displacement is measured on the shaft, so the bearing could be inaccessible or difficult to reach. In addition, the machine can be continuously monitored online. This conclusion allows for the future practical implementation of the method.

At the current stage of development, the method can only warn about the detection of bearing damage (the method cannot indicate the type of damage). Therefore, informing the maintenance staff about the need to carefully look at the bearing (when *blue* and *red* colors dominates) or to replace it (when the damage map is mostly *red* and *black*) becomes a possibility.

The next stages of the method developed in diagnosing bearings will be continued in subsequent articles.

Author Contributions: R.G.: Conceptualization, Investigation, Methodology, Project administration, Validation, Visualization, Writing—Original Draft, Funding acquisition, Resources, Supervision. B.B.: Data curation, Investigation, Resources, Software, Validation, Visualization, Writing—Reviewing and Editing, Funding acquisition. J.E.M.: Reviewing and Editing, Visualization, Funding acquisition. All authors have read and agreed to the published version of the manuscript.

Funding: The presented work was supported by the Ministry of Education and Science in Poland (research project No. WZ/WM-IIM/2/2022), by the Polish National Agency for Academic Exchange as part of the Academic International Partnerships (PPI/APM/2018/1/00033/U/001 project) and Erasmus+ Programme fund (partnership agreement 2017–3475/001–001).

Institutional Review Board Statement: Not applicable.

Informed Consent Statement: Not applicable.

Data Availability Statement: Not applicable.

Conflicts of Interest: The authors declare that they have no conflict of interest.

References

1. Ambrożkiewicz, B.; Syta, A.; Meier, N.; Litak, G.; Georgiadis, A. Radial internal clearance analysis in ball bearings. *Eksploat. I Niezawodn.—Maint. Reliab.* **2021**, *23*, 42–54. [CrossRef]
2. Boudiaf, A.; Moussaoui, A.; Dahane, A.; Atoui, I. A Comparative Study of Various Methods of Bearing Faults Diagnosis Using the Case Western Reserve University Data. *J. Fail. Anal. Prev.* **2016**, *16*, 271–284. [CrossRef]
3. Cerrada, M.; Sánchez, R.V.; Li, C.; Pacheco, F.; Cabrera, D.; Valente de Oliveira, J.; Vásquez, R.E. A review on data-driven fault severity assessment in rolling bearings. *Mech. Syst. Signal Process.* **2018**, *99*, 169–196. [CrossRef]
4. Gupta, P.; Pradhan, M.K. Fault detection analysis in rolling element bearing: A review. *Mater. Today Proc.* **2017**, *4*, 2085–2094. [CrossRef]
5. Huang, L.; Hu, N.; Yang, Y.; Chen, L.; Wen, J.; Shen, G. Study on Electromagnetic–Dynamic Coupled Modeling Method—Detection by Stator Current of the Induction Motors with Bearing Faults. *Machines* **2022**, *10*, 682. [CrossRef]

6. Islam, M.M.M.; Prosvirin, A.E.; Kim, J.M. Data-driven prognostic scheme for rolling-element bearings using a new health index and variants of least-square support vector machines. *Mech. Syst. Signal Process.* **2021**, *160*, 107853. [CrossRef]
7. Orhan, S.; Nizami, A.; Celik, V. Vibration monitoring for defect diagnosis of rolling element bearings as a predictive maintenance tool: Comprehensive case studies. *NDT E Int.* **2006**, *39*, 293–298. [CrossRef]
8. Satwara, N.; Patel, V.N. Vibration Monitoring of Defective Shaft Bearing System. In *Recent Advances in Machines and Mechanisms*; Gupta, V.K., Amarnath, C., Tandon, P., Ansari, M.Z., Eds.; Springer: Singapore, 2022.
9. Singh, M.; Shaik, A.G. Faulty bearing detection, classification and location in a three-phase induction motor based on Stockwell transform and support vector machine. *Measurement* **2019**, *131*, 524–533. [CrossRef]
10. Tengfei, Z.; Shuyong, L.; Sua, Z. Review on Fault Diagnosis on the Rolling Bearing. *J. Phys. Conf. Ser.* **2021**, *1820*, 012107.
11. Zarei, M.A.; Tajeddine, H.R.K. Vibration analysis for bearing fault detection and classification using an intelligent filter. *Mechatronics* **2014**, *24*, 151–157. [CrossRef]
12. Zheng, H.L.; Wang, R.X.; Yang, Y.T.; Yin, J.C.; Li, Y.B.; Li, Y.Q.; Xu, M.Q. Cross-domain fault diagnosis using knowledge transfer strategy: A review. *IEEE Access* **2019**, *7*, 129260–129290. [CrossRef]
13. Altaf, M.; Akram, T.; Khan, M.A.; Iqbal, M.; Ch, M.M.I.; Hsu, C.H. A New Statistical Features Based Approach for Bearing Fault Diagnosis Using Vibration Signals. *Sensors* **2022**, *22*, 2012. [CrossRef]
14. Hasan, M.J.; Kim, J.-M. Bearing Fault Diagnosis under Variable Rotational Speeds Using Stockwell Transform-Based Vibration Imaging and Transfer Learning. *Appl. Sci.* **2018**, *8*, 2357. [CrossRef]
15. Janjarasjitta, S.; Ocak, H.; Loparo, K.A. Bearing condition diagnosis and prognosis using applied nonlinear dynamical analysis of machine vibration signal. *J. Sound Vib.* **2008**, *317*, 112–126. [CrossRef]
16. Karacay, T.; Akturk, N. Experimental diagnostics of ball bearings using statistical and spectral methods. *Tribol. Int.* **2009**, *42*, 836–843. [CrossRef]
17. Khan, M.A.; Asad, B.; Kudelina, K.; Vaimann, T.; Kallaste, A. The Bearing Faults Detection Methods for Electrical Machines—The State of the Art. *Energies* **2023**, *16*, 296. [CrossRef]
18. Kudelina, K.; Baraškova, T.; Shirokova, V.; Vaimann, T.; Rassõlkin, A. Fault detecting accuracy of mechanical damages in rolling bearings. *Machines* **2022**, *10*, 86. [CrossRef]
19. Lei, Y. Fault diagnosis of rotating machinery based on empirical mode decomposition. In *Structural Health Monitoring. Smart Sensors, Measurement and Instrumentation*; Yan, R., Chen, X., Mukhopadhyay, S., Eds.; Springer: Cham, Switzerland, 2017; Volume 26, pp. 259–292.
20. Li, B.; Zhang, P.L.; Liu, D.S.; Mi, S.S.; Ren, G.Q.; Tian, H. Feature extraction for rolling element bearing fault diagnosis utilizing generalized S transform and two-dimensional non-negative matrix factorization. *J. Sound Vib.* **2011**, *330*, 2388–2399. [CrossRef]
21. Liu, Z.; Zhang, L. A review of failure modes, condition monitoring and fault diagnosis methods for large-scale wind turbine bearings. *Measurement* **2020**, *149*, 107002. [CrossRef]
22. López, C.; Naranjo, Á.; Lu, S.; Moore, K.J. Hidden Markov Model based Stochastic Resonance and its Application to Bearing Fault Diagnosis. *J. Sound Vib.* **2022**, *528*, 116890. [CrossRef]
23. Lu, S.; Zheng, P.; Liu, Y.; Cao, Z.; Yang, H.; Wang, Q. Sound-aided vibration weak signal enhancement for bearing fault detection by using adaptive stochastic resonance. *J. Sound Vib.* **2019**, *449*, 18–29. [CrossRef]
24. Muruganatham, B.; Sanjith, M.A.; Krishnakumar, B.; Satya Murtyk, S.A.V. Roller element bearing fault diagnosis using singular spectrum analysis. *Mech. Syst. Signal Process.* **2013**, *35*, 150–166. [CrossRef]
25. Patel, V.N.; Tandon, N.; Pandey, R.K. Defect detection in deep groove ball bearing in presence of external vibration using envelope analysis and Duffing oscillator. *Measurement* **2012**, *45*, 960–970. [CrossRef]
26. Peng, B.; Bi, Y.; Xue, B.; Zhang, M.; Wan, S. A Survey on Fault Diagnosis of Rolling Bearings. *Algorithms* **2022**, *15*, 347. [CrossRef]
27. Tandon, N.; Choudhury, A. A review of vibration and acoustic measurement methods for the detection of defects in rolling element bearings. *Tribol. Int.* **1999**, *32*, 469–480. [CrossRef]
28. Tiboni, M.; Remino, C.; Bussola, R.; Amici, C. A Review on Vibration-Based Condition Monitoring of Rotating Machinery. *Appl. Sci.* **2022**, *12*, 972. [CrossRef]
29. Wu, D.; Wang, J.; Wang, H.; Liu, H.; Lai, L.; He, T.; Xie, T. An Automatic Bearing Fault Diagnosis Method Based on Characteristics Frequency Ratio. *Sensors* **2020**, *20*, 1519. [PubMed]
30. Al-Dossary, S.; Raja Hamzah, R.I.; Mba, D. Observations of changes in acoustic emission waveform for varying seeded defect sizes in a rolling element bearing. *Appl. Acoust.* **2009**, *70*, 58–81. [CrossRef]
31. Al-Ghamd, A.M.; Mba, D. A comparative experimental study on the use of acoustic emission and vibration analysis for bearing defect identification and estimation of defect size. *Mech. Syst. Signal Process.* **2006**, *20*, 1537–1571. [CrossRef]
32. Pham, M.T.; Kim, J.-M.; Kim, C.H. Intelligent Fault Diagnosis Method Using Acoustic Emission Signals for Bearings under Complex Working Conditions. *Appl. Sci.* **2020**, *10*, 7068. [CrossRef]
33. Chao, J.; Bo, W.; Youmin, H. Heat generation modeling of ball bearing based on internal load distribution. *Tribol. Int.* **2012**, *45*, 8–15.
34. Cristea, A.F.; Pascovici, M.; Fillon, M. Clearance and lubricant selection for avoiding seizure in a circumferential groove journal bearing based on a lumped model analysis. *Mech. Ind.* **2011**, *12*, 399–408. [CrossRef]
35. Takabi, J.; Khonsari, M.M. Experimental testing and thermal analysis of ball bearings. *Tribol. Int.* **2013**, *60*, 93–103. [CrossRef]

36. Arun, P.; Lincon, S.A.; Prabhakaran, N. Non-intrusive detection and characterization of bearing faults from the temporal features of vibration. *Aust. J. Mech. Eng.* **2020**, *18* (Suppl. S1), S132–S139. [CrossRef]
37. Kecik, K.; Smagala, A.; Lyubitska, K. Ball Bearing Fault Diagnosis Using Recurrence Analysis. *Materials* **2022**, *15*, 5940. [CrossRef]
38. Rai, A.; Upadhyay, S.H. A review on signal processing techniques utilized in the fault diagnosis of rolling element bearings. *Tribol. Int.* **2016**, *96*, 289–306. [CrossRef]
39. Wen, J.; Khonsari, M.M.; Huad, Y. Three-dimensional heat transfer analysis of pin-bushing system with oscillatory Motion: Theory and experiment. *J. Tribol.-Trans. Asme* **2011**, *133*, 011101. [CrossRef]
40. Cai, J.H.; Xiao, Y.L. Bearing fault diagnosis method based on the generalized s transform time-frequency spectrum de-noised by singular value decomposition. *Proc. Inst. Mech. Eng. Part C J. Mech. Eng. Sci.* **2019**, *233*, 2467–2477. [CrossRef]
41. Chandra, N.H.; Sekhar, A.S. Fault detection in rotor bearing systems using time frequency techniques. *Mech. Syst. Signal Process.* **2016**, *72–73*, 105–133. [CrossRef]
42. Dhamande, L.S.; Chaudhari, M.B. Compound gear-bearing fault feature extraction using statistical features based on timefrequency method. *Measurement* **2018**, *125*, 63–77. [CrossRef]
43. Feng, Z.P.; Liang, M.; Chu, F.L. Recent advances in time-frequency analysis methods for machinery fault diagnosis: A review with application examples. *Mech. Syst. Signal Process.* **2013**, *38*, 165–205. [CrossRef]
44. Sun, G.D.; Yang, X.; Xiong, C.Y.; Hu, Y.; Liu, M.Y. Rolling bearing fault diagnosis based on time-frequency compression fusion and residual time-frequency mixed attention network. *Appl. Sci.* **2022**, *12*, 4831. [CrossRef]
45. Rai, V.K.; Mohanty, A.R. Bearing fault diagnosis using FFT of intrinsic mode functions in Hilbert-Huang transform. *Mech. Syst. Signal Process.* **2007**, *6*, 2607–2615. [CrossRef]
46. Wang, R.; Fang, H.; Yu, L.; Yu, L.; Chen, J. Sparse and low-rank decomposition of the time-frequency representation for bearing fault diagnosis under variable speed conditions. *ISA Trans.* **2022**, *128*, 579–598. [CrossRef]
47. Zhang, Z.; Wang, Y.; Wang, K. Fault diagnosis and prognosis using wavelet packet decomposition, Fourier transform and artificial neural network. *J. Intell. Manuf.* **2013**, *24*, 1213–1227. [CrossRef]
48. Zheng, K.; Luo, J.F.; Zhang, Y.; Li, T.L.; Wen, J.F.; Xiao, H. Incipient fault detection of rolling bearing using maximum autocorrelation impulse harmonic to noise deconvolution and parameter optimized fast eemd. *ISA Trans.* **2019**, *89*, 256–271. [CrossRef]
49. Wang, L.; Liu, Z.; Miao, Q.; Zhang, X. Time-frequency analysis based on ensemble local mean decomposition and fast kurtogram for rotating machinery fault diagnosis. *Mech. Syst. Signal Process.* **2018**, *103*, 60–75. [CrossRef]
50. Wang, L.; Shao, Y. Fault feature extraction of rotating machinery using a reweighted complete ensemble empirical mode decomposition with adaptive noise and demodulation analysis. *Mech. Syst. Signal Process.* **2020**, *138*, 106545. [CrossRef]
51. Liu, Y.; Jiang, Z.; Haizhou, H.; Xiang, J. Asymmetric penalty sparse model based cepstrum analysis for bearing fault detections. *Appl. Acoust.* **2020**, *165*, 107288. [CrossRef]
52. Ma, J.; Wu, J.; Wang, X.; Fan, Y.; Leng, T. A fault detection method of rolling bearing based on wavelet packet-cepstrum. *Res. J. Appl. Sci.* **2013**, *5*, 3402–3406. [CrossRef]
53. Verma, A.; Srivastava, S. Review on condition monitoring techniques oil analysis, thermography and vibration analysis. *Int. J. Enhanc. Res. Sci. Technol. Eng.* **2014**, *3*, 18–25.
54. Lee, J.; Kim, H. Development of enhanced Wigner–Ville distribution function. *Mech. Syst. Signal Process.* **2001**, *15*, 367–398. [CrossRef]
55. Safizadeh, M.S.; Lakis, A.A.; Thomas, M. Time-frequency algorithms and their applications. *Int. J. Comput. Appl.* **2000**, *7*, 167–186.
56. Quinde, I.R.; Sumba, J.C.; Ochoa, L.E.; Guevara, A.J.V.; Morales-Menendez, R. Bearing fault diagnosis based on optimal timefrequency representation method. *IFAC-Pap.* **2019**, *52*, 194–199.
57. Peter, W.T.; Peng, Y.H.; Yam, R. Wavelet analysis and envelope detection for rolling element bearing fault diagnosis-their affectivities and flexibilities. *J. Vib. Acoust.* **2001**, *123*, 303–310.
58. Unal, M.; Onat, M.; Demetgul, M.; Kucuk, H. Fault diagnosis of rolling bearings using a genetic algorithm optimized neural network. *Measurement* **2015**, *58*, 187–196. [CrossRef]
59. Han, D.Y.; Li, P.; An, S.J.; Shi, P.M. Multi-frequency weak signal detection based on wavelet transform and parameter compensation band-pass multi-stable stochastic resonance. *Mech. Syst. Signal Process.* **2016**, *70–71*, 995–1010. [CrossRef]
60. Liang, P.; Wang, W.; Yuan, X.; Liu, S.; Zhang, L.; Cheng, Y. Intelligent fault diagnosis of rolling bearing based on wavelet transform and improved ResNet under noisy labels and environment. *Eng. Appl. Artif. Intell.* **2022**, *115*, 105269. [CrossRef]
61. Malhotra, A.; Minhas, A.M.; Singh, S.; Zuo, M.J.; Kumara, R.; Kankar, P.K. Bearing fault diagnosis based on flexible analytical wavelet transform and fuzzy entropy approach. *Mater. Today Proc.* **2021**, *43*, 625–635. [CrossRef]
62. Wang, W.; Zhao, Y.; Yi, C.; Tsui, K.L.; Lin, J. Sparsity guided empirical wavelet transform for fault diagnosis of rolling element bearings. *Mech. Syst. Signal Process.* **2018**, *101*, 290–308. [CrossRef]
63. Chen, Z.; Mauricio, A.; Li, W.; Gryllias, K. A deep learning method for bearing fault diagnosis based on cyclic spectral coherence and convolutional neural networks. *Mech. Syst. Signal Process.* **2020**, *140*, 106683. [CrossRef]
64. Dibaj, A.; Hassannejad, R.; Ettefagh, M.M. Incipient fault diagnosis of bearings based on parameter-optimized VMD and envelope spectrum weighted kurtosis index with a new sensitivity assessment threshold. *ISA Trans.* **2020**, *114*, 413–433. [CrossRef]
65. Gao, S.; Xu, L.; Zhang, Y.; Pei, Z. Rolling bearing fault diagnosis based on SSA optimized self-adaptive DBN. *ISA Trans.* **2021**, *128*, 485–502. [CrossRef]

66. Hakim, M.; Omran, A.A.B.; Ahmed, A.N.; Al-Waily, M.; Abdellatif, A. A systematic review of rolling bearing fault diagnoses based on deep learning and transfer learning: Taxonomy, overview, application, open challenges, weaknesses and recommendations. *Ain Shams Eng. J.* **2022**, *14*, 101945. [CrossRef]
67. Hasan, M.J.; Islam, M.M.M.; Kim, J.-M. Bearing Fault Diagnosis Using Multidomain Fusion-Based Vibration Imaging and Multitask Learning. *Sensors* **2022**, *22*, 56. [CrossRef]
68. Li, G.; Deng, C.; Wu, J.; Xu, X.; Shao, X.; Wang, Y. Sensor Data-Driven Bearing Fault Diagnosis Based on Deep Convolutional Neural Networks and S-Transform. *Sensors* **2019**, *19*, 2750. [CrossRef]
69. Liu, R.; Yang, B.; Zio, E.; Chen, X. Artificial intelligence for fault diagnosis of rotating machinery: A review. *Mech. Syst. Signal Process.* **2018**, *108*, 33–47. [CrossRef]
70. Ma, J.; Dong, S.; Chen, G.; Peng, P.; Qian, L. A data-driven normal contact force model based on artificial neural network for complex contacting surfaces. *Mech. Syst. Signal Process.* **2021**, *156*, 107612. [CrossRef]
71. Mao, W.; Feng, W.; Liu, Y.; Zhang, D.; Liang, X. A new deep auto-encoder method with fusing discriminant information for bearing fault diagnosis. *Mech. Syst. Signal Process.* **2021**, *150*, 107233. [CrossRef]
72. Neupane, D.; Seok, J. Bearing Fault Detection and Diagnosis Using Case Western Reserve University Dataset With Deep Learning Approaches: A Review. *IEEE Access* **2020**, *8*, 93155–93178. [CrossRef]
73. Sohaib, M.; Kim, C.H.; Kim, J.M. A hybrid feature model and deep-learning-based bearing fault diagnosis. *Sensors* **2017**, *17*, 2876. [CrossRef]
74. Toma, R.N.; Prosvirin, A.E.; Kim, J.M. Bearing fault diagnosis of induction motors using a genetic algorithm and machine learning classifiers. *Sensors* **2020**, *20*, 1884. [CrossRef]
75. Xu, Y.; Deng, Y.; Ma, C.; Zhang, K. The Enfigram: A robust method for extracting repetitive transients in rolling bearing fault diagnosis. *Mech. Syst. Signal Process.* **2021**, *158*, 107779. [CrossRef]
76. Yin, A.; Yan, Y.; Zhang, Z.; Li, C.; Sánchez, R.-V. Fault Diagnosis of Wind Turbine Gearbox Based on the Optimized LSTM Neural Network with Cosine Loss. *Sensors* **2020**, *20*, 2339. [CrossRef]
77. Zeng, W.; Li, M.; Yuan, C.; Wang, Q.; Liu, F.; Wang, Y. Classification of focal and non-focal EEG signals using empirical mode decomposition (EMD), phase space reconstruction (PSR) and neural networks. *Artif. Intell. Rev.* **2019**, *52*, 625–647. [CrossRef]
78. Zhang, J.; Wu, J.; Hu, B.; Tang, J. Intelligent fault diagnosis of rolling bearings using variational mode decomposition and self-organizing feature map. *J. Vib. Control* **2020**, *26*, 1866–1897. [CrossRef]
79. Zhang, X.; Zhao, B.; Lin, Y. Machine Learning Based Bearing Fault Diagnosis Using the Case Western Reserve University Data: A Review. *IEEE Access* **2021**, *9*, 155598–155608.
80. Zhang, Y.; Xing, K.; Bai, R.; Sun, D.; Meng, Z. An enhanced convolutional neural network for bearing fault diagnosis based on time–frequency image. *Measurement* **2020**, *157*, 107667. [CrossRef]
81. Lindstedt, P.; Kotowski, A. Basics for innovations in vibroacoustic diagnostics of transport machilles rotor blades. *Arch. Transp.* **2004**, *16*, 47–61.
82. Kotowski, A.; Lindstedt, P. The using of signals of impulse acoustic response in tests of rotor blades in stationary conditions. In Proceedings of the 4th International Symposium: Stability Control of Rotating Machinery ISCORMA-4, Calgary, AB, Canada, 27–31 August 2007; pp. 160–169.
83. Lindstedt, P.; Rokicki, E.; Borowczyk, H.; Majewski, P. Application of the correlation function and Fourier trans-formation to evaluation of technical condition demonstrated by blade sof a rotor machine during the operation process. *J. KONES Powertrain Transp.* **2009**, *16*, 2.
84. Lindstedt, P.; Rokicki, E.; Borowczyk, H.; Majewski, P. Rotor blades condition monitoring method based on the elimination of the environment signal. *Res. Work. AFIT* **2009**, *25*, 15–24. [CrossRef]
85. Lindstedt, P.; Grądzki, R. Parametrical models of working rotor machine blade diagnostics with its unmesurable en-vironment elimination. *Acta Mech. Autom.* **2010**, *4*, 56–63.
86. Grądzki, R. Parametric Diagnostic Models of the Blades of a Working Rotary Machine with the Elimination of Non-Mesurable Environmental Signals. Ph.D. Thesis, Bialystok University of Technology, Bialystok, Poland, 2012.
87. Grądzki, R.; Lindstedt, P.; Kulesza, Z.; Bartoszewicz, B. Rotor blades diagnosis method based on differences in phase shifts. *Shock Vib.* **2018**, *2018*, 9134607. [CrossRef]
88. Grądzki, R.; Lindstedt, P.; Kulesza, Z.; Bartoszewicz, B. Assessment of rotor blades stationarity condition based on differences in phase shifts. *Eng. Fail. Anal.* **2020**, *118*, 104874. [CrossRef]
89. Gradzki, R.; Kulesza, Z.; Bartoszewicz, B. Method of shaft crack detection based on squared gain of vibration amplitude. *Nonlinear Dyn.* **2019**, *98*, 671–690. [CrossRef]
90. Technical Specification SKF Bearings. Available online: https://www.skf.com/us/products/rolling-bearings/ball-bearings/self-aligning-ball-bearings/productid-1207%20EKTN9 (accessed on 11 January 2023).